https://doi.org/10.30758/0555-2648-2021-67-2-147-164
УДК 551.5

ОРИГИНАЛЬНАЯ СТАТЬЯ ORIGINAL ARTICLE

EVALUATION OF COASTAL ANTARCTIC PRECIPITATION IN LMDZ6 GLOBAL ATMOSPHERIC MODEL USING GROUND-BASED RADAR OBSERVATIONS

FLORENTIN LEMONNIER[1,2], ALIZÉE CHEMISON[3], GERHARD KRINNER[4], JEAN-BAPTISTE MADELEINE[1], CHANTAL CLAUD[1], CHRISTOPHE GENTHON[1]*

[1] — *Sorbonne Université, École normale supérieure, PSL Research University, École polytechnique, CNRS, Laboratoire de Météorologie dynamique, LMD/IPSL, F-75005 Paris, France*

[2] — *Escape Productions, F-75004 Paris, France*

[3] — *Laboratoire des Sciences du Climat et de l'Environnement, CNRS-CEA-UVSQ – UMR8212, CE Saclay, France*

[4] — *Université Grenoble Alpes, CNRS, Institut des Géosciences de l'Environnement, Grenoble, France*

contact@escape-productions.com

Summary

In the current context of climate change in the poles, one of the objectives of the APRES3 (Antarctic Precipitation Remote Sensing from Surface and Space) project was to characterize the vertical structure of precipitation in order to better simulate it. Precipitation simulated by models in Antarctica is currently very widespread and it overestimates the data. Sensitivity studies have been conducted using a global climate model and compared to the observations obtained at the Dumont d'Urville coast station, obtained by a Micro Rain Radar (MRR). The LMDz/IPSL general circulation model, with zoomed configuration over Dumont d'Urville, has been considered for this study. A sensitivity study was conducted on the physical and numerical parameters of the LMDz model with the aim of estimating their contribution to the precipitation simulation. Sensitivity experiments revealed that changes in the sedimentation and sublimation parameters do not significantly impact precipitation rate. However, dissipation of the LMDz model, which is a numerical process that dissipates spatially excessive energy and keeps the model stable, impacts precipitation indirectly but very strongly. A suitable adjustment of the dissipation reduces significantly precipitation over Antarctic peripheral area, thus providing a simulated profile in better agreement with the MRR observations.

Keywords: Antarctic precipitation, General Circulation Model evaluation, numerical dissipation evaluation, polar climate modeling.

For Citation: *Lemonnier F., Chemison A., Krinner G., Madeleine J.-B., Claud C., Genthon C.* Evaluation of coastal Antarctic precipitation in LMDz6 global atmospheric model using ground-based radar observations. *Problemy Arktiki i Antarktiki.* Arctic and Antarctic Research. 2021, 67 (2): 147–164. https://doi.org/10.30758/0555-2648-2021-67-2-147-164.

Received 09.06.2021 **Revised 25.06.2021** **Accepted 28.06.2021**

ОЦЕНКА ОСАДКОВ В ПРИБРЕЖНЫХ РАЙОНАХ АНТАРКТИКИ В ГЛОБАЛЬНОЙ МОДЕЛИ АТМОСФЕРЫ LMDZ6 С ИСПОЛЬЗОВАНИЕМ НАЗЕМНЫХ РАДИОЛОКАЦИОННЫХ НАБЛЮДЕНИЙ

Ф. ЛЕМОНЬЕ[1,2], А. ШЕМИСО[3], Г. КРИНЕР[4], Ж.-Б. МАДЕЛАН[1], Ш. КЛО[1], К. ЖЕНТОН[1]*

[1] — *Лаборатория динамической метеорологии, LMD/IPSL, Университет Сорбонна, Высшая нормальная школа, Политехническая школа, Парижский исследовательский университет, НЦНИ, Париж, Франция*

[2] — *Эскейп Продакшнс, Париж, Франция*

[3] — *Лаборатория наук о климате и окружающей среде, НЦНИ, Комиссариат по атомной энергии и альтернативным энергиям, Версальский университет «Сен-Кантен-ан-Ивелин», Сакле, Франция*

[4] — *Университет Гренобль Альпы, НЦНИ, Институт наук о Земле, Гренобль, Франция*

contact@escape-productions.com

Резюме

В текущем тренде изменения климата на полюсах одна из задач проекта APRES3 (Дистанционное зондирование осадков в Антарктике с поверхности и из космоса) заключается в том, чтобы уточнить вертикальную структуру осадков и повысить качество их прогноза. Известные результаты моделирования осадков в Антарктиде базируются на данных с высокой степенью неопределенности и сильно разнятся. Исследование избирательной чувствительности расчета осадков проводилось на основе глобальной климатической модели и сопоставлялось с наблюдениями, полученными с помощью метеорадара (MRR) на береговой станции Дюмон-д'Юрвиль. Использовалась LMDz/IPSL-модель общей циркуляции с повышенной детализацией в районе станции Дюмон-д'Юрвиль. Была выполнена оценка вклада физических и численных параметров данной модели в расчет осадков. Вычислительные эксперименты показали, что изменения параметров седиментации и сублимации не влияют существенно на прогнозируемую скорость выпадения осадков. Однако диссипация, возникающая в модели LMDz в процессе вычислений, рассеивая пространственно избыточную энергию и обеспечивая устойчивость модели, хотя и косвенно, но очень сильно влияет на рассчитываемую величину осадков. Адекватная подгонка уровня рассеивания при моделировании значительно снижает количество осадков в периферийных районах Антарктики, обеспечивая таким образом лучшее согласование моделируемого профиля с данными метеорадарных наблюдений.

Ключевые слова: антарктические осадки, моделирование полярного климата, оценка численной диссипации, оценка модели общей циркуляции.

Для цитирования: *Lemonnier F., Chemison A., Krinner G., Madeleine J.-B., Claud C., Genthon C.* Evaluation of coastal Antarctic precipitation in LMDz6 global atmospheric model using ground-based radar observations. *Problemy Arktiki i Antarktiki.* 2021, 67 (2): 147–164. https://doi.org/10.30758/0555-2648-2021-67-2-147-164.

Поступила 09.06.2021 **После переработки 25.06.2021** **Принята 28.06.2021**

1. INTRODUCTION

Between 1880 and 2012, the Earth's mean global temperature increased by 0.85 ± 0.2 °C, and this warming is predicted to intensify during the 21st century. As temperatures warm, sea level rises as continental ice melts and the oceans expand thermally. Sea levels have already increased by 190 ± 20 mm between 1901 and 2010 and the Antarctic contribution is estimated at 0.27 mm·yr^{-1} [1]. Antarctica has already lost

2720 ± 1390 billion tonnes of ice between 1992 and 2017 [2]. To understand the impact of the Antarctic ice cap on mean sea level, it is essential to calculate its mass balance.

Precipitation represents the only positive contribution of the surface mass balance, but is difficult to assess over this continent. Precipitation estimates are inferred from surface accumulation observations during field campaigns, but is affected by high wind speeds over the ice-sheet leading to under-estimation of the snow accumulation [3]. It is also observed from space with the CloudSat satellite [4] and recent studies have greatly improved confidence in the results of this satellite [5, 6]. However, the observations are unavailable below 1200 meters above the surface due to contamination of radar reflections by icy surfaces [7]. There are also in-situ observations of precipitation measurements and snow accumulation. However, field campaigns allowing this are difficult to be conducted and are mainly located near the coast [8].

Climate models are used to analyze and understand dynamical and physical processes, such as precipitation, and then to predict the future climate of Antarctica. Different types of climate models exist, ranging from basic 1D models to meso-scale and coupled global climate models. These models provide a better understanding of the current climate with its fluctuations, as well as a prediction of future climate change. This ability to predict climate change makes it a particularly interesting tool, notably for the Coupled Model Intercomparison Project (CMIP, [9]) in the current context of global warming. These models have different uses, depending on whether they are global or regional, as well as different levels of complexity and various horizontal and vertical resolutions. The calculation time is crucial, so a regional model can easily include developed and complex physical processes, while a global model has to provide suitable simulations in any region of the globe thus limiting the complexity of the processes it integrates.

Most climate models predict that the Antarctic ice sheet surface mass balance is subject to increase due to higher precipitation rate, which is itself associated with an increase in atmospheric temperature [10]. This change in precipitation ranges from 5.5 to 24.4 % during the 21st century, depending on greenhouse gas emissions scenarios. However, the Palerme et al. [11] and Roussel et al. [12] studies presenting an intercomparison of CMIP5 and CMIP6 models with CloudSat observations and ERA-Interim reanalysis shows that the models overestimate precipitation in comparison with CloudSat climatology [4], sometimes by more than 100 %. And even though the simulated surface precipitation is compared to an observation level at an altitude of 1200 meters above the local surface, the discrepancy between data and models is large, and questionable for the future prediction of precipitation. In addition, the agreement between data and models is even worse for the simulation of precipitation on the plateau than over the peripheral regions [11–12].

Since November 2015, during a field campaign at the French base in Dumont d'Urville, instruments have been installed, including a Micro Rain Radar (MRR) observing clouds and precipitation particles from surface [13]. This instrument has provided a continuous vertical structure of precipitation and its climatology. Among other results, this has highlighted the sublimation of precipitation by katabatic winds, as well as providing information on the mean sedimentation rate of precipitation [14–15]. This vertical profile is also an excellent tool for evaluating the simulated vertical structure of precipitation.

In this study, we propose to evaluate the vertical structure of precipitation at Dumont d'Urville, simulated by the general circulation model LMDz [16, 17], using the MRR dataset. This model is the atmospheric component of the coupled IPSL model.

This model having different degrees of complexity because of different uses, it is important to verify how precipitation is simulated by itself, and especially to verify if the vertical profile of precipitation is in agreement with the observed profile. In section 2, the model configuration and the ground radar observations are presented to do this study. The sensitivity experiments performed on each configuration of the LMDz model and their results are discussed in section 3. Then, an exploration of numerical dissipation in the LMDz model applied to temperature and its impact in simulated precipitation is discussed in section 4. Finally, we conclude this study in section 5.

2. METHODS

2.1. The LMDz-IPSL climate model

The LMDz dynamical core is based on finite difference and finite volume discretization of the primitive equations of meteorology and transport equations, coupled to a set of physical parameterizations [16,17]. The radiative transfer scheme is the Rapid Radiative Transfer Model (RRTM) from [18]. Clouds are predicted by a statistical cloud scheme which is described in detail in Madeleine et al. [17]. Regarding the microphysics of cold clouds, a fraction f_{iw} of the condensed water qc is assumed to be frozen, depending on the temperature between 273.15 K where $f_{iw} = 0$ and 243.15 K where $f_{iw} = 1$. Then a fraction of the condensed water is partially precipitated according to Zender and Kiehl [19]. The associated sink of cloud water is:

$$\frac{dq_{iw}}{dt} = \frac{1}{\rho}\frac{\partial}{\partial z}\left(\rho_{wi} w q_{iw}\right), \quad (1)$$

where $w_{iw} = \gamma_{iw} \cdot w_0$, $w_0 = 3.29(\rho q_{iw})^{0.16}$ being the characteristic sedimentation rate of ice crystals given by Heymsfield and Donner [20] depending on the solid cloud water and γ_{iw} being a tunable parameter. Precipitation is then re-evaporated and included into the vapor water following:

$$\frac{dP}{dz} = \beta\left(1 - \frac{q}{q_{sat}}\right)\sqrt{P}, \quad (2)$$

where P is the precipitation flux and β is a tunable parameter.

This model configuration only admits the atmospheric model, without taking into account vegetation or ocean circulation models. However, there is a surface scheme. It is composed of four categories: oceans, continental surfaces, sea-ice and glaciers. The surface fluxes are calculated by taking into account the parameters of each type of surface. Regarding thermal conduction of the ice cap and surface properties, the albedo in the near IR is 0.68 and 0.96 in the visible, the thermal inertia is 2000 $J \cdot m^{-2} \cdot K^{-1} \cdot s^{-1/2}$, which is a typical value of pure ice [21]. In order to have the better resolution possible above Dumont d'Urville with a GCM, the model is stretched longitudinally and latitudinally, reaching a horizontal resolution of ~25 km. We nudged the LMDz model with wind, temperature and humidity extracted from ERA-Interim reanalysis with a 6-hours time-step outside the zoom. It is nudge-free inside the zoomed area [22]. This allows us to use the full physics, not influenced by the nudging tendencies, inside the zoomed region while having at the same time the best atmospheric conditions outside this zoomed region.

The model has 79 vertical levels in its current configuration, with refinement in the boundary layer troposphere. The vertical precipitation profile studied at Dumont d'Urville

in the LMDz model is selected over continental surface. A spin-up of 4 months is necessary to balance the model, then each simulation is conducted for one month corresponding to our dataset period.

2.2. Micro Rain Radar (MRR) observations

The MRR is a vertically profiling Doppler radar operating at a frequency of 24.3 GHz (K-band) and having a beamwidth of 2° (around 50 m in diameter at 3000 m). The vertical resolution is set to 100 m per bin ranging from 300 – first valid available measurements – to 3000 m [13]. The MRR's raw measurement – Doppler spectral densities – are available at 10s temporal resolution then minute averaged. The collected data are processed using the IMProTool developed by Maahn and Kollias [23]. The radar reflectivity derived from MRR was calibrated by comparison with a colocated X-band polarimetric radar over the period from December 2015 to January 2016 (for more details, see [13]. Through this calibration with the second radar, the reflectivity (at X-band) is converted into snowfall rates using a radar reflectivity *Ze*/20 snowfall rate *Sr* relation [13] :

$$Ze = 76 \cdot S_r^{0.91}, \quad (3)$$

with *Ze* the radar reflectivity (in dBZ) and Sr the snowfall rate (in mm/hr). Grazioli et al. [13], proposed a range of values of [69–83] for the prefactor and [0.78–1.09] for the exponent corresponding to a confidence interval of 95 %.

The period selected for this study is February 2017. During this period precipitation events are particularly frequent with different amplitudes and durations. Rather than studying a particular event, we focus on the monthly accumulation of precipitation at each vertical level of the MRR. The monthly accumulation of precipitation is presented in Figure 1. The sublimated part of the precipitation can be clearly observed below 1000 meters, due to katabatic winds [14].

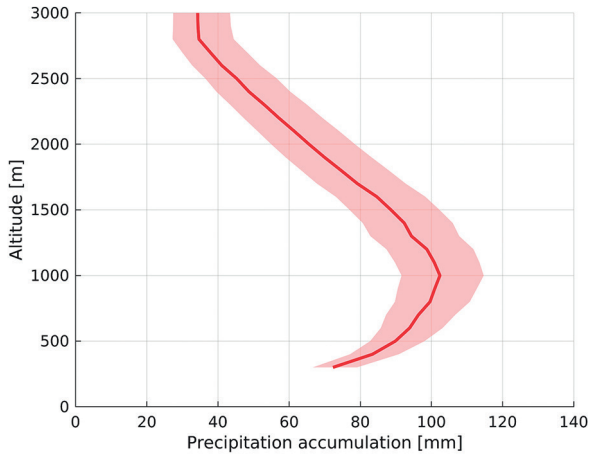

Fig. 1. Vertical precipitation accumulation over the February 2017 period recorded by the MRR. Red filled area corresponds to the 95 % confidence interval of the MRR observations

Рис. 1. Вертикальное накопление осадков за февраль 2017 г., зарегистрированное метеорадаром. Область, закрашенная красным, соответствует 95 % доверительному интервалу наблюдений метеорадара

2.3. Description of sensitivity experiments

Models are very sensitive to horizontal resolution, as the consideration of many parameterizations will strongly depend on it. We used different dimensions of the grids as well as the size of the domain under study. Two domains are presented: the first is 250 km × 250 km, the second is 1000 km × 1000 km, and they are called respectively SMALL and BIG. These areas are presented in Figure 2, the maps are at the size of the zoomed region of the BIG simulation and the red frames represent the size of the zoomed region of the SMALL simulation. We evaluated the horizontal resolution of LMDz by performing simulations on two zoomed domains of different sizes. Indeed, when zooming with the LMDz model, the zoomed region can be widened. The size of the "SMALL" zoom domain in LMDz allows the model to adapt its own physics inside the zoom in an environment where large-scale wind, temperature and humidity advections are controlled by ERA-Interim reanalyses. The 5 second configuration with a BIG domain is larger, so the model can have its own mesocyclonic circulations within the zoom. The center of the zoom is in this case not very affected by the ERA-Interim reanalysis.

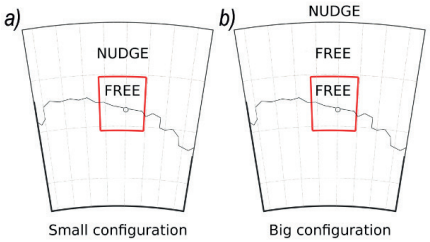

Fig. 2. Representation of the LMDz SMALL (*a*) and BIG (*b*) domains

Рис. 2. Представление МАЛОГО (*a*) и БОЛЬШОГО (*b*) доменов в модели LMDz

The first sensitivity experiment is evaluating the feedback of the LMDz model to the extent of the nudged-free zoomed domain. Indeed, in the case where the zoom area is restricted in size, the center of the zoom is very sensitive to forcing outside this area. This case is similar to a regional climate model. Inversely, when the zoom area is large, the center of the zoom area is less affected by the forcings imposed on it from the outside and the model is more like a global climate model in a free configuration.

The second experiment studies the sensitivity of solid precipitation to sedimentation velocity rate. To do so, we have tested different values of the parameter w_{iw} in the equation 1 through its parameter γ_{iw}. The different imposed values are summarized in Table 1.

It is important to note the difference between experiment *SedEx* 02 whose sedimentation rate tends towards 1 m·s^{-1} and the experiment *SedEx* 03 which sedimentation

Table 1

Sedimentation rate experiments on LMDz precipitation simulation

Таблица 1

Эксперименты по скорости седиментации при моделировании осадков в LMDz

Experiment	Sedimentation rate, m·s^{-1}
Control simulation	$\gamma_{iw} w_0 \rightarrow 0.25$
SedEx 01	$\gamma_{iw} w_0 \rightarrow 0.5$
SedEx 02	$\gamma_{iw} w_0 \rightarrow 1$
SedEx 03	$\gamma_{iw} w_0 = 1$

Table 2

Sublimation tunable parameter experiments on LMDz precipitation evaporation

Таблица 2

Эксперименты с настраиваемыми параметрами сублимации по испарению осадков в модели LMDz

Experiment	β sublimation parameter
Control simulation	$\beta = 2 \cdot 10^{-4}$
SubEx 01	$\beta = 4 \cdot 10^{-4}$
SubEx 02	$\beta = 8 \cdot 10^{-4}$
SubEx 03	$\beta = 2 \cdot 10^{-3}$

rate is equal to 1 $m \cdot s^{-1}$ (see equation 1). Indeed, the value of w_0 is varying with qiw and the air density as a function of pressure and temperature. In the *SedEx* 03 experiment, this variation is not taken into account.

The third sensitivity study with LMDz has been performed on the precipitation sublimation equation 2. To do this, several orders of magnitude have been fixed to β tunable parameter value. These values are summarized in the table 2.

3. RESULTS OF SENSITIVITY EXPERIMENTS

3.1. Horizontal resolution in LMDz

We have evaluated two horizontal configurations of LMDz with different sizes of the zoomed domain. The SMALL configuration is a zoomed domain with a size of 250 × 250 km and the BIG configuration is a zoomed domain with a size of 1000 × 1000 km. It is important

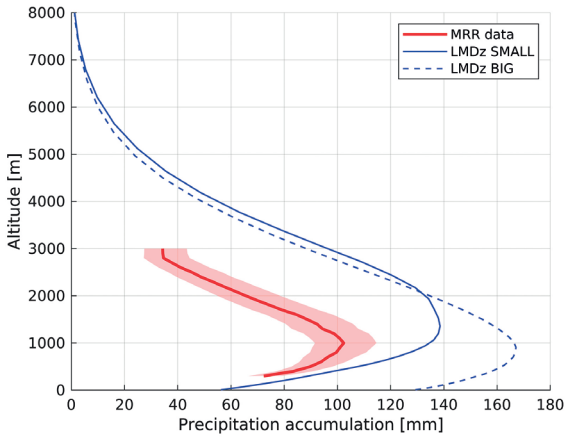

Fig. 3. Precipitation profiles simulated with LMDz and compared with MRR observations. Blue solid line corresponds to LMDz configuration with a SMALL zoomed domain. Blue dashed line correspond to LMDz configuration with a BIG zoomed domain. Red solid line is the observed MRR vertical profile of precipitation accumulation and red filled area corresponds to the 95 % confidence interval of the MRR observations

Рис. 3. Сопоставление профилей осадков, рассчитанных по модели LMDz, с наблюдениями метеорадара. Синяя сплошная линия соответствует зуму конфигурации LMDz для МАЛОГО домена. Синяя пунктирная линия — зум конфигурации LMDz для БОЛЬШОГО домена. Красная сплошная линия представляет собой вертикальный профиль накопления осадков по данным метеорадара; закрашенная красным область соответствует 95 % доверительному интервалу наблюдений метеорадара

to note that there is the same horizontal resolution inside the zoom. Figure 3 shows the accumulation profiles at Dumont d'Urville resulting from this experiment. The BIG simulation produces a high precipitation accumulation on the surface with 130 mm compared to 55 mm for the SMALL simulation. The two simulated precipitation profiles overestimate the observed accumulation profile. The maximum before inversion of the BIG simulation is below 1000 m, which is in accordance with the observations. The maximum precipitation of the SMALL simulation is at a higher altitude, at 1200 m.

3.2. LMDz microphysical parameterizations

Considering that the SMALL configuration of the LMDz model is in better agreement with observations than BIG configuration (see Figure 3), and that the large-scale advected fields are well known thanks to ERA-Interim reanalysis, we performed this experiment in order to evaluate the physics of the model only. Figure 4 presents sensitivity experiments summarized in Tables 1 and 2, in comparison with MRR vertical observed precipitation accumulation profile. The surface precipitation rate appears to be in agreement with the MRR at 300 m. However, the amount of simulated precipitation is far too high in all experiments. The maximum precipitation reached by the MRR exceeds 100 mm of accumulation at 1000 m, while the model simulates almost 50 mm more. Moreover, precipitation variations in the simulated profiles, either for the sedimentation rate experiment or the sublimation experiment, are small.

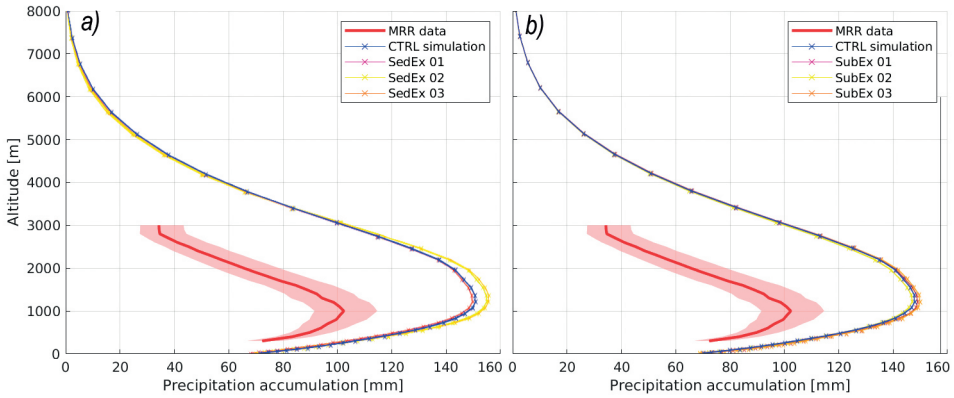

Fig. 4. Precipitation accumulation profiles of SMALL LMDz simulations. Red solid line is the observed MRR vertical profile of precipitation accumulation and red filled area corresponds to the 95 % confidence interval of the MRR observations. Blue solid line corresponds to the standard LMDz zoomed configuration with a 25 km horizontal resolution and a SMALL domain. Purple, yellow and orange solid lines correspond to sensitivity experiments summarized in Table 1 for (*a*) and in Table 2 for (*b*)

Рис. 4. Профили накопления осадков для МАЛОГО домена в модели LMDz. Красная сплошная линия представляет собой вертикальный профиль накопления осадков по данным метеорадара; закрашенная красным область соответствует 95 % доверительному интервалу наблюдений метеорадара. Синяя сплошная линия соответствует МАЛОМУ домену при стандартной детализации модели LMDz с горизонтальным разрешением 25 км. Сплошные пурпурная, желтая и оранжевая линии соответствуют вычислительным экспериментам с параметрами, представленными в таблицах 1 (*a*) и 2 (*b*)

3.3. Discussion on the resolution and the microphysics

Figure 3 shows a significant difference in the amount of simulated precipitation between BIG and SMALL LMDz simulations. One of the zoomed regions being small and its circulation very sensitive to ERA-Interim reanalysis while the other being big enough to allow mesoscale circulations to develop without influence from ERA-Interim reanalysis, we verified if the temperature and humidity fields are at the origin of this difference. Figures 5*a* and 5*b* present the absolute difference in potential temperature at 950 hPa and 500 hPa respectively between SMALL simulation and BIG simulation. Figures 5*c* and 5*d* present the absolute difference in specific humidity at 950 hPa and

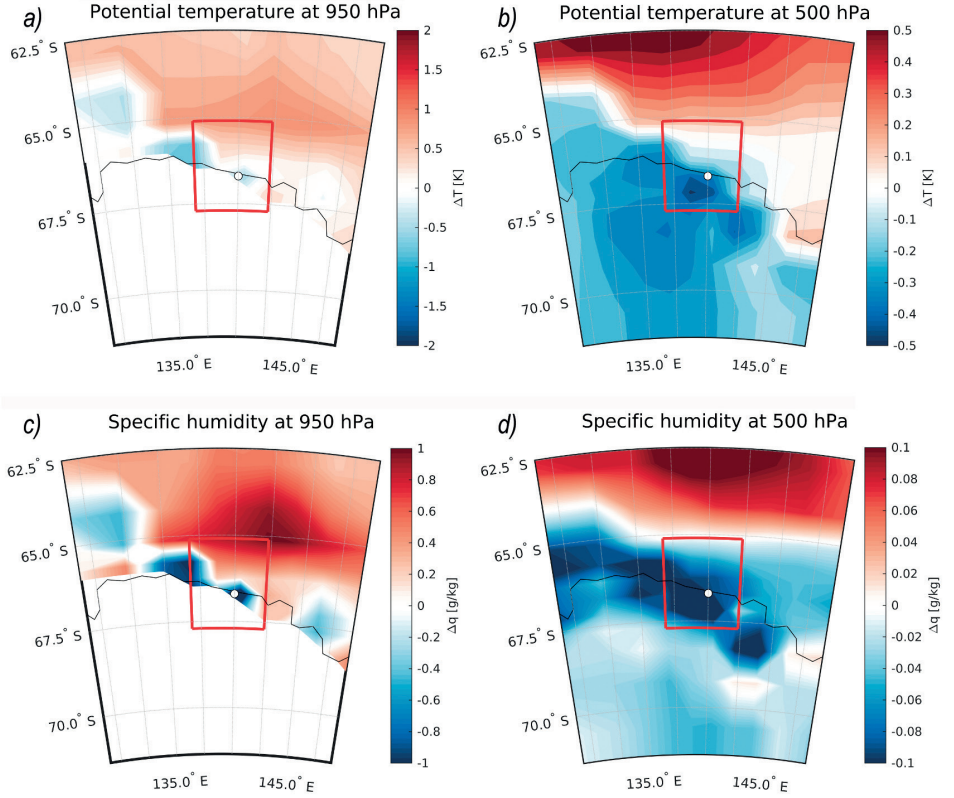

Fig. 5. Difference of potential temperature in LMDz between SMALL and BIG simulations: at 950 hPa (*a*); at 500 hPa (*b*). Difference of specific humidity between SMALL and BIG simulations: at 950 hPa (*c*); at 500 hPa (*d*). The zoomed area of the SMALL domain is represented by the red frame and the zoomed area of the BIG domain is represented by the size of the map. The colours range from blue to red. When the SMALL configuration overestimates a variable compared to the BIG configuration, the color is red

Рис. 5. Различие потенциальной температуры в расчетах LMDz для МАЛОГО и БОЛЬШОГО доменов: при 950 гПа (*a*); аналогичные результаты при 500 гПа (*b*). Различие удельной влажности для МАЛОГО и БОЛЬШОГО доменов: при 950 гПа (*c*); аналогичные результаты при 500 гПа (*d*). Область детализации МАЛОГО домена ограничена красной рамкой, а область детализации БОЛЬШОГО домена совпадает с размерами карты. Цвета палитры изменяются от синего до красного. Когда в случае малой конфигурации значение какой-либо характеристики завышается по сравнению с большой, цвет становится красным

500 hPa respectively between SMALL simulation and BIG simulation. For the SMALL simulation, the wind, temperature and humidity trends outside the zoomed region are constrained by ERA-Interim. This means that outside the red frame, the BIG simulation is closely following ERA-Interim reanalysis. Concerning the temperature, the model in its BIG configuration is warmer than the SMALL configuration over the continent and colder over the ocean. There is clearly a more humid air mass above Dumont d'Urville in the BIG simulation. And in a general way, the continent and the ocean region along the coasts are moister in the BIG simulation, with a correlation between temperature and humidity. This shows that mesoscale circulations in the LMDz model redistribute quantities of potential temperature and humidity, thus concentrating moisture along the coasts, as seen on Figures 5*c* and 5*d*, with a warm bias over the Antarctic continent, as seen on Figure 5*a* and 5*b*.

Sensitivity tests on the microphysics of LMDz have shown that it has almost no impact on the amount of simulated precipitation. In addition, the amount of simulated precipitation overestimates by approximately 50 % the amount of precipitation observed along the vertical profile at Dumont d'Urville. The existing microphysics of the LMDz model does not balance first order warm and moist biases for the representation of polar solid precipitation.

4. EXPLORING THE IMPACT OF LMDZ NUMERICAL DISSIPATION ON PRECIPITATION

LMDz, like many GCM, implements a dissipation scheme to prevent the accumulation of energy at scales close to the grid resolution. These accumulations of energy appear when GCM is not resolving turbulent scales at the grid resolution [24, 25]. In the LMDz model, it involves a spatial displacement of dynamic or thermal fields, which can induce, for example, local warming or a variation in dynamics created by purely numerical processes. Thus, a model that is too dissipative may generate precipitation that has no physical relevance.

The dissipation is expressed in LMDz as an iterated Laplacian term on a given variable ψ as follows:

$$\left[\frac{d\psi}{dt}\right]_{dissip} = \frac{(-1)^{q_d+1} l_{\min}^{2q_d}}{\tau^{\psi}} \nabla^{2q_d} \psi, \qquad (4)$$

where q_d is the order of dissipation and τ^{ψ} the damping timescale associated with the variable ψ at the smallest spatial scale 10 l_{min}, depending on the horizontal resolution of the model. q_d is an iterative operator, it acts as a filter on the spatial resolution. When $q_d = 1$, the process is overly dissipative on circulations at large scales and at higher values, dissipation occurs more at the grid scale than at the large scale. Large values of τψ means weaker dissipation. Indeed, τ^{ψ} represents the time to dissipate a perturbation on variable ψ developing at the spatial scale l_{min}. The three variables designated by ψ are vorticity and divergence of winds, and potential temperature. They are chosen to set horizontal dissipation on the rotational component of the dynamic flows (qdrot and τrot, i.e. Rossby waves), its divergent component (q_d^{div} and τ^{div}, i.e. gravity waves) and the diabatic perturbations (q_d^{h} and τ_h i.e. latent heat of condensation, rain re-evaporation, snow sublimation, ...).

In LMDz, and more generally in the GCMs methodology, qd and τψ are determined empirically. A trade-off between model stability, damping energy at the smallest scales and minimizing impact on the large-scale flows is sought. There are general rules for refining the dissipation parameters for LMDz, with qd ranging between 1 and 4, and τψ taking values ranging between one and two hours for a 0.5° – 1° GCM simulation. The standard configuration of the LMDz model uses as dissipation values $q_d^{div} = 1$, $q_d^{rot} = 2$, $q_d^{h} = 2$ as operators and $\tau^{div} = 600$ s, $\tau^{rot} = 1200$ s, $\tau^{h} = 1200$ s as timescales.

4.1. Sensitivity experiments results

In order to study and understand the impact of the different dissipation parameters on precipitation, we have performed sensitivity tests that are summarized in the table 3. For all sensitivity tests, the resulting simulations are less dissipative than the control simulation. The corresponding vertical precipitation accumulation profiles are shown in the Figure 6. These experiments were performed on the two configurations of the LMDz under consideration, the results and behaviors are similar but we will only present those performed on the SMALL configuration, which has a precipitation profile closer to the observed profile (see Figure 3).

Table 3

Dissipation parameter experiments on SMALL LMDz precipitation

Таблица 3

Эксперименты с параметрами диссипации для малого домена в модели LMDz

Experiment	q_d parameter	τ parameter
D01	$q_d^{div} = 2$	–
D02	$q_d^{rot} = 4$	–
D03	$q_d^{h} = 4$	–
D04	–	$\tau^{div} = 1200$s
D05	–	$\tau^{rot} = 2400$s
D06	–	$\tau^{h} = 2400$s
D07	$q_d^{div} = 2$; $q_d^{rot} = 4$; $q_d^{h} = 4$	–
D08	–	$\tau^{div} = 1200$ s; $\tau^{rot} = 2400$ s; $\tau^{h} = 2400$ s
D09	$q_d^{div} = 2$; $q_d^{rot} = 4$; $q_d^{h} = 4$	$\tau^{div} = 1200$ s; $\tau^{rot} = 2400$ s; $\tau^{h} = 2400$ s
D10	$q_d^{div} = 2$; $q_d^{rot} = 4$	$\tau^{div} = 1200$ s; $\tau^{rot} = 2400$ s
D11	$q_d^{h} = 4$	$\tau^{h} = 2400$ s

Note. The values displayed in the table correspond only to tested parameters. When a parameter is not modified, its value corresponds to the standard parameters of LMDz and it is not displayed.

In a general way, sensitivity experiments on and parameters have little impact on precipitation. The same applies to the τ^{div} and τ^{rot} parameters. However, the dissipation applied to the parameter τ^{h} has a strong impact on the dissipation profile, as observed on the simulations D03, D06 and D11. For the D07 simulation, where all q_d parameters are modified, it can be deduced that the excellent agreement between the simulated and observed precipitation is due mainly to the modifications on diabatic perturbations.

Finally, the D09 experiment best reproduces the MRR observations. Indeed, the simulated profile is very close to the observed profile and within the confidence range of the instrument.

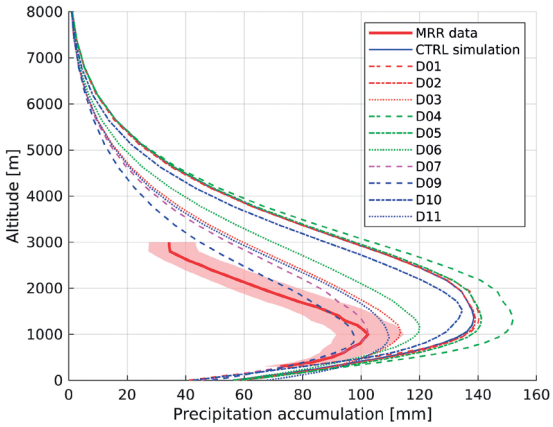

Fig. 6. Precipitation accumulation profiles of LMDz. Red solid line is the observed MRR vertical profile of precipitation accumulation and red filled area corresponds to the 95 % confidence interval of the MRR observations. Blue solid line is the standard LMDz simulation, the red lines represent the experiments on the q_d operators, green lines represent the experiments on the damping timescale τ parameter. Purple and blue dashed and dotted lines represent experiments on combinations between q_d and τ

Рис. 6. Профили накопления осадков по модели LMDz. Красная сплошная линия представляет собой вертикальный профиль, зарегистрированный метеорадаром, а закрашенная красным область соответствует 95 % доверительному интервалу полученных данных. Синяя сплошная линия — стандартный результат моделирования, красные линии соответствуют вычислительным экспериментам на основе q_d операторов, зеленые линии — расчеты по демпфированию параметра временной шкалы τ. Пурпурные и синие, штриховые и пунктирные линии — результаты комбинирования характеристик q_d и τ

4.2. Discussion on the dissipation adjustment

In order to study and understand how dissipation affects precipitation, we have investigated the time series of temperatures of the control simulation and the D09 simulation with the best results relative to the MRR observations. They are presented in the Figure 7. The impact of the dissipation is mainly visible at low altitude, where the control model is about 3 °C warmer than the D09 simulation. In addition, when a precipitation event occurs (e.g., February 1, 10, 14, and 21), the control simulation is warmer than the D09 simulation, which can result in higher precipitation rates being triggered by higher temperature gradients and moister atmospheric masses.

In order to understand the behaviour of the dissipation on a spatial scale, we averaged the temperatures over the month of February according to a transect from Dumont d'Urville (140° E 66.7° S) to Dome C (123.2° E 75° S), showed in Figure 8. When time series are averaged and projected over a larger spatial scale, there is a geographic reorganization of temperature in the less dissipative simulation. In the D09 simulation, the area above Dumont d'Urville is on average colder than in the control simulation. This is due to warmer temperature fields over ocean regions that are less laterally diffused over Antarctic coastal regions.

As shown in Figure 9, as the atmosphere cools over the peripheral regions of Antarctica, air masses become less humid and this has a strong impact on precipitation by concentrating it over ocean regions. Thus, the variation in precipitation observed in

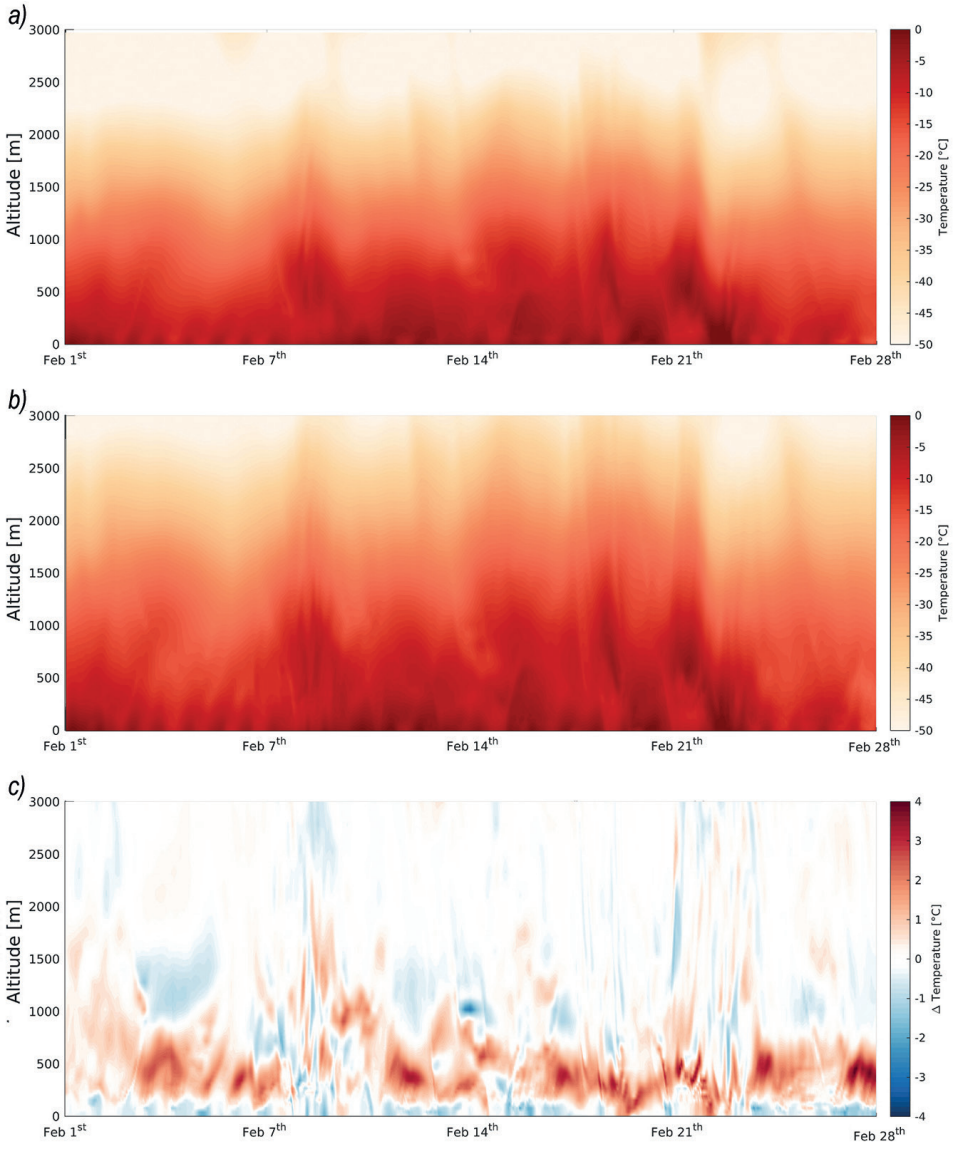

Fig. 7. Temperature time series of over the February 2017 period: control experiment (*a*); D09 experiment (*b*); differential time series of temperature between control and D09 simulations (*c*).

The colors range from blue to red. When the control configuration of the model overestimates temperature compared to the D09 simulation, the color used is red

Рис. 7. Временные температурные ряды за февраль 2017 г.: для контрольного эксперимента (*a*); для вычислительного эксперимента D09 (*b*); дифференциальный временной ряд отклонений температуры между контрольным расчетом и экспериментом D09 (*c*).

Когда конфигурация управления модели завышает температуру по сравнению с симуляцией D09, используется красный цвет

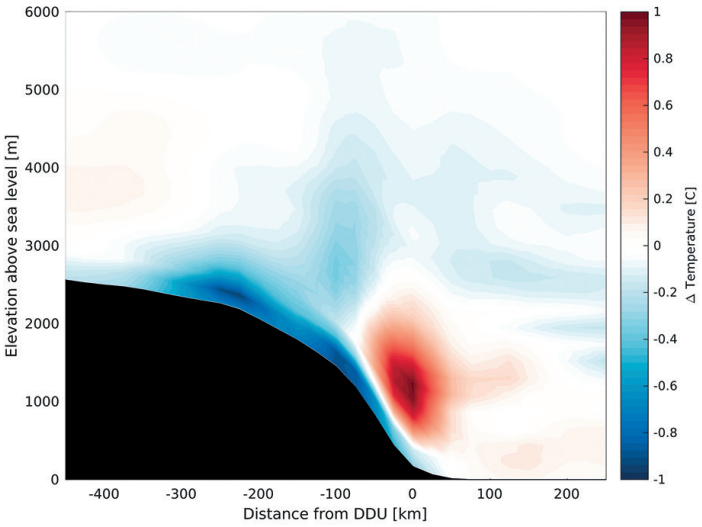

Fig. 8. Differential averaged temperature between control and D09 simulations along a Dumont d'Urville (140° E 66.7° S) – Dome C (123.2° E 75° S) Dome C transect.

The colors range from blue to red. When the control configuration of the model overestimates temperature compared to the D09 simulation, the color used is red

Рис. 8. Различие в усредненной температуре контрольного расчета и эксперимента D09 вдоль разреза Дюмон д'Юрвиль (140° E 66,7° S) – Купол С (123,2° E 75° S). Цвета варьируют от синего до красного.

Когда конфигурация управления модели завышает температуру по сравнению с симуляцией D09, используется красный цвет

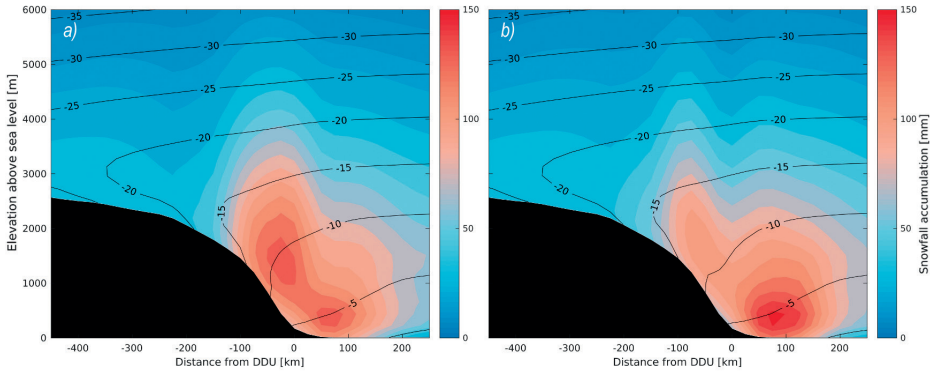

Fig. 9. Average precipitation over the February 2017 period along a Dumont d'Urville (140° E 66.7° S) – Dome C (123.2° E 75° S) transect: in the control LMDz simulation (*a*), in the D09 LMDz simulation.

The black lines represent the average isotherms

Рис. 9. Среднее количество осадков за февраль 2017 г. на разрезе Дюмон-д'Юрвиль (140° E 66,7° S) – Купол С (123,2° E 75° S): при контрольном моделировании LMDz (*a*), для варианта расчета D09 (*b*).

Черные линии представляют собой средние изотермы.

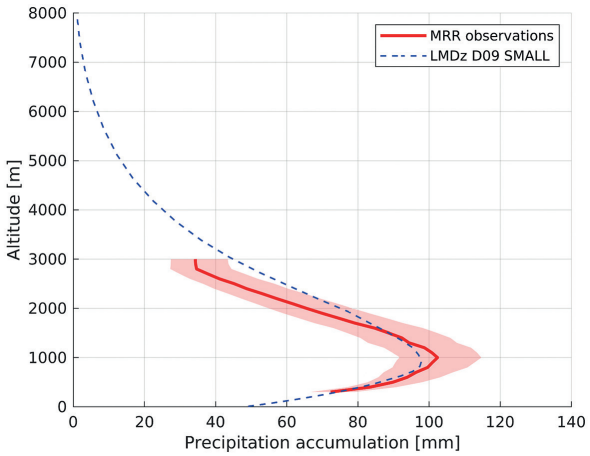

Fig. 10. Precipitation accumulation profiles of MRR and LMDz. Red solid line is the observed MRR vertical profile of precipitation accumulation and red filled area corresponds to the 95 % confidence interval of the MRR observations. Blue dashed line is the D09 LMDz simulation

Рис. 10. Профили накопления осадков по данным метеорадара и модели LMDz. Красная сплошная линия представляет собой наблюдаемый метеорадаром вертикальный профиль накопления осадков, закрашенная красным область соответствует 95 % доверительному интервалу наблюдений метеорадара. Синяя пунктирная линия — прогноз LMDz в эксперименте D09

the Figure 6 corresponds to a horizontal redistribution of precipitation in a less dissipative configuration of the LMDz model.

When comparing the MRR observations with the D09 simulation of the LMDz model, as shown on Figure 10, the average vertical evolution of precipitation is consistent between the model and the data. This result is interesting because it shows that a model whose microphysics is simplified to satisfy a global issue can correctly simulate solid precipitation in the Antarctic region. The LMDz model only contains a precipitation autoconversion equation and a snowfall resublimation equation, but this allows the climate in Dumont d'Urville to be accurately represented during the month of February 2017, and in particular for the katabatic inversion of precipitation. The LMDz model is too dissipative in its control version, but the dissipation adjustment takes priority over the microphysics adjustment and this allows precipitation to be redistributed over oceanic rather than continental regions.

5. CONCLUSION

Comparison of the vertical precipitation profile observed at Dumont d'Urville with the general circulation model LMDz provided a new perspective on precipitation modelling in the polar regions. We evaluated a global model in several zoomed configurations over Dumont d'Urville station in order to compare the simulated precipitation profile by testing its microphysics and its numerical dissipation settings with ground radar observations.

Variations in microphysical parameters related to LMDz precipitation have a small impact on the simulated precipitation profile. However, LMDz is very sensitive to the size of its zoomed region as well as to the advections of large-scale fields of winds, temperatures and humidity of ERA-Interim reanalysis. Indeed, in a large domain, where the model is able to generate its own mesoscale circulation, moisture is concentrated above

Dumont d'Urville area and warm and moist bias is generated over the continent near the coasts (blue patterns on Fig. 5*d*). This is not an expected outcome. When a correct general circulation is forced by configuring a small zoomed region where the centre of the zoom remains influenced by the ERA-Interim reanalysis and by improving the GCM dissipation adjustment in a less dissipative way, the model generates a precipitation profile at Dumont d'Urville that is in excellent agreement with the observed profile.

Numerical parameters that guarantee the stability of a model, such as dissipation, often require empirical adjustments. Dissipation being applied in cases of excess energy to be diffused at the mesh scale, the large-scale currents are not significantly affected by this numerical setting. Thus, the use of observations such as local precipitation rather than large-scale field can be an excellent tool for the fine-tuning of the dissipation of a model, as illustrated here with the LMDz model. This study showed that a better adjusted GCM model such as LMDz is correct for assessing the climate over polar regions and provide an additional element to the major problem of calculating the mass balance in Antarctica.

6. CODE AND DATA AVAILABILITY

Data from the Micro Rain Radar at Dumont d'Urville station have been obtained with the logistical support of the French Polar institute IPEV (program CALVA) and are available at https://doi.pangaea.de/10.1594/PANGAEA.882565. The LMDz model is available from http://web.lmd.jussieu.fr/trac (last access: 9 January 2020). Due to the size of the high-frequency outputs (several To of simulation outputs) of the LMDz, only simulations of the small domain of the LMDz are available: https://doi.pangaea.de/10.1594/PANGAEA.917641.

Author contributions. FL led the analysis and drafted the paper. JBM, CC, HG, GK and CG supervised the project. FL ran the LMDz simulations. AC analyzed the simulated precipitation profiles. All authors discussed the results and commented on the paper.

Competing interests. The authors declare no conflict of interest.

Funding. This work was supported by the French National Research Agency (Grant number: ANR-15-CE01-0003).

Acknowledgements. The authors thank Karine Marquois, Philippe Weil and the IT department of the Laboratoire de Météorologie Dynamique / Institut Pierre Simon Laplace for the informatics support. The authors thank Frédéric Hourdin and Sébastien Froment for their valuable advices. CG acknowledges support by the French polar institute IPEV under projects CALVA and APRES3 for MRR radar deployement and operation at DDU station.

REFERENCES

1. *Church J.A., Clark P.U., Cazenave A., Gregory J.M., Jevrejeva S., Levermann A., Merrifield M. A., Milne G.A., Nerem, R.S., Nunn P. D., Payne A., Pfeffer W.T., Stammer D., Unnikrishnan A.S.* Sea-level rise by 2100. Science. 2013, 342: 1445–1445.

2. *Shepherd A., Ivins E., Rignot E., Smith B., Van Den Broeke M., Velicogna I., Whitehouse P., Briggs K., Joughin I., Krinner G., Nowicki S., Payne T., Scambos T., Schlegel N., Geruo A., Agosta C., Ahlstrøm A., Babonis G., Barletta V., ... Wouters B.* Mass balance of the Antarctic Ice Sheet from 1992 to 2017. Nature. 2018, 558: 219–222.

3. *Das I., Bell R.E., Scambos T.A., Wolovick M., Creyts T.T., Studinger M., Frearson N., Nicolas J.P., Lenaerts J.T., van den Broeke M.R.* Influence of persistent wind scour on the surface mass balance of Antarctica. Nature Geoscience. 2013, 6 (5): 367–371.

4. *Palerme C., Kay J., Genthon C., L'Ecuyer T., Wood N., Claud C.* How much snow falls on the Antarctic ice sheet? The Cryosphere. 2014, 8: 1577–1587.

5. *Souverijns N., Gossart A., Lhermitte S., Gorodetskaya I.V., Grazioli J., Berne A., Duran-Alarcon C., Boudevillain B., Genthon C., Scarchilli C., van Lipzig N.P.M.* Evaluation of the CloudSat surface snowfall product over Antarctica using ground-based precipitation radars. The Cryosphere. 2018, 12: 3775–3789. https://doi.org/10.5194/tc-12-3775-2018.

6. *Lemonnier F., Madeleine J., Claud C., Genthon C., Durán-Alarcón C., Palerme C., Berne A., Souverijns N., van Lipzig N., Gorodetskaya I., L'Ecuyer T., Wood N.* Evaluation of CloudSat snowfall rate profiles by a comparison with in-situ micro rain radars observations in East Antarctica. The Cryosphere. 2019, 13 (3): 943–954.

7. *Palerme C., Claud C., Wood N., L'Ecuyer T., Genthon C.* How does ground clutter affect CloudSat snowfall retrievals over ice sheets? IEEE Geoscience And Remote Sensing Letters. 2019, 16: 342–346.

8. *Eisen O., Frezzotti M., Genthon C., Isaksson E., Magand O., van den Broeke M.R., Dixon D.A., Ekaykin A., Holmlund P., Kameda T., Karlof L., Kaspari S., Lipenkov V.Y., Oerter H., Takahashi S., Vaughan D.G.* Ground-based measurements of spatial and temporal variability of snow accumulation in East Antarctica. Reviews of Geophysics. 2008, 46(RG2001), doi:10.1029/2006RG000218.

9. *Taylor K.E., Stouffer R.J., Meehl G.A.* An overview of CMIP5 and the experiment design. Bulletin of the American Meteorological Society. 2012, 93: 485–498.

10. *Krinner G., Guicherd B., Ox K., Genthon C., Magand O.* Influence of oceanic boundary conditions in simulations of Antarctic climate and surface mass balance change during the coming century. Journal of Climate. 2008, 21: 938–962.

11. *Palerme C., Genthon C., Claud C., Kay J.E., Wood N.B., L'Ecuyer T.* Evaluation of current and projected Antarctic precipitation in CMIP5 models. Climate Dynamics. 2017, 48: 225–239.

12. *Roussel M.-L., Lemonnier F., Genthon C., Krinner G.* Evaluating Antarctic precipitation in ERA5 and CMIP6 10 against CloudSat observations. The Cryosphere. 2020, 14: 2715–2727.

13. *Grazioli J., Genthon C., Boudevillain B., Duran-Alarcon C., Del Guasta M., Jean-Baptiste M., Berne A.* Measurements of precipitation in Dumont d'Urville, Adélie Land, East Antarctica. The Cryosphere. 2017, 11: 1797–1811.

14. *Grazioli J., Madeleine J.-B., Gallée H., Forbes R. M., Genthon C., Krinner G., Berne A.* Katabatic winds diminish precipitation contribution to the Antarctic ice mass balance. Proceedings of the National Academy of Sciences. 2017, 114: 10858–10863.

15. *Durán-Alarcón C., Boudevillain B., Genthon C., Grazioli J., Souverijns N., van Lipzig N.P.M., Gorodetskaya I.V., Berne A.* The vertical structure of precipitation at two stations in East Antarctica derived from micro rain radars. The Cryosphere. 2019, 13: 247–264.

16. *Hourdin F., Rio C., Grandpeix J.-Y., Madeleine J.-B., Cheruy F., Rochetin N., Jam A., Musat I., Idelkadi A., Fairhead L., Foujols M.-A., Mellul L., Traore A.-K., Dufresne J.-L., Boucher O., Lefebvre M.-P., Millour E., Vignon E., Jouhaud J., Diallo F.B., Lott F., Gastineau G., Caubel A., Meurdesoif Y., Ghattas J.* LMDZ6A: the atmospheric component of the IPSL climate model with improved and better tuned physics. Journal of Advances in Modeling Earth Systems. 2020, 12 (7): e2019MS001892.

17. *Madeleine J.-B., Hourdin F., Grandpeix J.-Y., Rio C., Dufresne J.-L., Vignon E., Boucher O., Konsta D., Cheruy F., Musat I., Idelkadi A., Fairhead L., Millour E., Lefebvre M.-P., Mellul L., Rochetin N., Lemonnier F., Touzé-Peiffer L., Bonazzola M.* Improved representation of clouds in the atmospheric component LMDZ6A of the IPSL-CM6A Earth System Model. Journal of Advances in Modeling Earth Systems. 2020, 12 (10): e2020MS002046.

18. *Mlawer E.J., Taubman S.J., Brown P.D., Iacono M.J., Clough S.A.* Radiative transfer for inhomogeneous atmospheres: RRTM, a validated correlated-k model for the longwave. Journal of Geophysical Research: Atmospheres. 1997, 102: 16663–16682.

19. *Zender C.S., Kiehl J.* Sensitivity of climate simulations to radiative effects of tropical anvil structure. Journal of Geophysical Research: Atmospheres. 1997, 102: 23793–23803.

20. *Heymsfield A.J., Donner L.J.* A scheme for parameterizing ice-cloud water content in general circulation models. Journal of the Atmospheric Sciences. 1990, 47: 1865–1877.

21. *Vignon E., Hourdin F., Genthon C., Gallée H., Bazile E., Lefebvre M.-P., Madeleine J.-B., Van de Wiel B.J.* Antarctic boundary layer parametrization in a general circulation model: 1-D simulations facing summer observations at Dome C. Journal of Geophysical Research: Atmospheres. 2017, 122: 6818–6843.

22. *Coindreau O., Hourdin F., Haeffelin M., Mathieu A., Rio C.* Assessment of physical parameterizations using a global climate model with stretchable grid and nudging. Monthly weather review. 2007, 135: 1474–1489.

23. *Maahn M., Kollias P.* Improved Micro Rain Radar snow measurements using Doppler spectra post-processing. Atmos. Meas. Tech. 2012, 5: 2661– 2673.

24. *Jablonowski C., Williamson D.L.* The pros and cons of diffusion, filters and fixers in atmospheric general circulation models. In: Lauritzen P., Jablonowski C., Taylor M., Nair R. (eds) Numerical Techniques for Global Atmospheric Models. Lecture Notes in Computational Science and Engineering, vol 80. Springer, Berlin, Heidelberg, 2011: 381–493.

25. *Spiga A., Guerlet S., Millour E., Indurain M., Meurdesoif Y., Cabanes S., Dubos T., Leconte J., Boissinot A., Lebonnois S., Sylvestre M., Fouchet T.* Global climate modeling of Saturn's atmosphere. Part II: multi-annual high-resolution dynamical simulations. Icarus, Elsevier. 2020, 335: 113377. 10.1016/j.icarus.2019.07.011. hal-02278447.